ISSN 1063-7761, Journal of Experimental and Theoretical Physics, 2018, Vol. 126, No. 1, pp. 132–145. © Pleiades Publishing, Inc., 2018.
Original Russian Text © E.Yu. Aristova, A.A. Aushev, V.K. Baranov, I.A. Belov, S.A. Bel'kov, A.Yu. Voronin, I.N. Voronich, R.V. Garanin, S.G. Garanin, K.G. Gainullin, A.G. Golubinskii, A.V. Gorodnichev, V.A. Denisova, V.N. Derkach, V.S. Drozhzhin, I.A. Ericheva, N.V. Zhidkov, R.I. Il'kaev, A.A. Krayukhin, A.G. Leonov, D.N. Litvin, K.N. Makarov, A.S. Martynenko, V.I. Malinov, V.V. Mis'ko, V.G. Rogachev, A.N. Rukavishnikov, E.A. Salatov, Yu.V. Skorochkin, G.Yu. Smorchkov, A.L. Stadnik, V.A. Starodubtsev, P.V. Starodubtsev, R.R. Sungatullin, N.A. Suslov, T.I. Sysoeva, V.Yu. Khatunkin, E.S. Tsoi, O.N. Shubin, V.N. Yufa, 2018, published in Zhurnal Eksperimental'noi i Teoreticheskoi Fiziki, 2018, Vol. 153, No. 1, pp. 157–172.

STATISTICAL, NONLINEAR, AND SOFT MATTER PHYSICS

Laser Simulations of the Destructive Impact of Nuclear Explosions on Hazardous Asteroids

E. Yu. Aristova[a], A. A. Aushev[a], V. K. Baranov[a], I. A. Belov[a], S. A. Bel'kov[a], A. Yu. Voronin[a], I. N. Voronich[a], R. V. Garanin[a], S. G. Garanin[a], K. G. Gainullin[a], A. G. Golubinskii[a], A. V. Gorodnichev[a], V. A. Denisova[a], V. N. Derkach[a], V. S. Drozhzhin[a], I. A. Ericheva[a], N. V. Zhidkov[a], R. I. Il'kaev[a], A. A. Krayukhin[a], A. G. Leonov[b], D. N. Litvin[a], K. N. Makarov[b], A. S. Martynenko[a], V. I. Malinov[a], V. V. Mis'ko[a], V. G. Rogachev[a], A. N. Rukavishnikov[a], E. A. Salatov[a], Yu. V. Skorochkin[a], G. Yu. Smorchkov[a], A. L. Stadnik[a], V. A. Starodubtsev[a], P. V. Starodubtsev[a,*], R. R. Sungatullin[a], N. A. Suslov[a], T. I. Sysoeva[a], V. Yu. Khatunkin[a], E. S. Tsoi[a], O. N. Shubin[c], and V. N. Yufa[b]

[a] *Russian Federal Nuclear Center—VNIIEF, Sarov, Nizhegorodskaya oblast, 607190 Russia*

[b] *Federal State Autonomous Higher Education Institution "Moscow Institute of Physics and Technology," Dolgoprudnyi, Moscow oblast, 141701 Russia*

[c] *State Atomic Energy Corporation "Rosatom," ul. Bol'shaya Ordynka 24, Moscow, 119017 Russia*

**e-mail: drdeceiver@gmail.com*

Received September 3, 2017

Abstract—We present the results of preliminary experiments at laser facilities in which the processes of the undeniable destruction of stony asteroids (chondrites) in space by nuclear explosions on the asteroid surface are simulated based on the principle of physical similarity. We present the results of comparative gasdynamic computations of a model nuclear explosion on the surface of a large asteroid and computations of the impact of a laser pulse on a miniature asteroid simulator confirming the similarity of the key processes in the full-scale and model cases. The technology of fabricating miniature mockups with mechanical properties close to those of stony asteroids is described. For mini-mockups 4–10 mm in size differing by the shape and impact conditions, we have made an experimental estimate of the energy threshold for the undeniable destruction of a mockup and investigated the parameters of its fragmentation at a laser energy up to 500 J. The results obtained confirm the possibility of an experimental determination of the criteria for the destruction of asteroids of various types by a nuclear explosion in laser experiments. We show that the undeniable destruction of a large asteroid is possible at attainable nuclear explosion energies on its surface.

DOI: 10.1134/S1063776118010132

1. INTRODUCTION

The collision with a large asteroid is one of the greatest catastrophes for our planet. Its impact can surpass in force and consequences other, more frequent natural catastrophes, such as the eruptions of volcanos or big earthquakes. Today humanity has achieved a sufficiently high level of technological development and can consider the possibility of preventing or mitigating the asteroid hazard in earnest. The threat of the intersection of the orbits of large bodies with the Earth's trajectory is predictable and potentially hazardous objects are being detected at present [1–3].

There are two approaches to the possible active protection of the Earth from hazardous cosmic objects: a change in the trajectory of asteroids [4–7] and the fragmentation of asteroids into small (nonhazardous) debris [8–10]. A shortcoming of the first approach is that the impact is comparatively weak and a long time interval is required for a significant deflection of the object [7], implying a very high accuracy of the advance prediction of a collision. Obviously, both factors are important in practice. When realizing the second approach, some of the debris will fly past the Earth, while some of them, especially of small sizes, will be destroyed and burn up in its atmosphere.

Let us make some approximate estimates of protection from asteroids. Let the asteroid–Earth encounter velocity be $V_{ast} \approx 20$ km s^{-1}, as with the Chebarkul meteorite. We will take the velocity that the fragments gain as the asteroid is fragmented by the nuclear explosion to be $V_{frag} \approx 10$ m s^{-1}. A nuclear explosion at a dis-

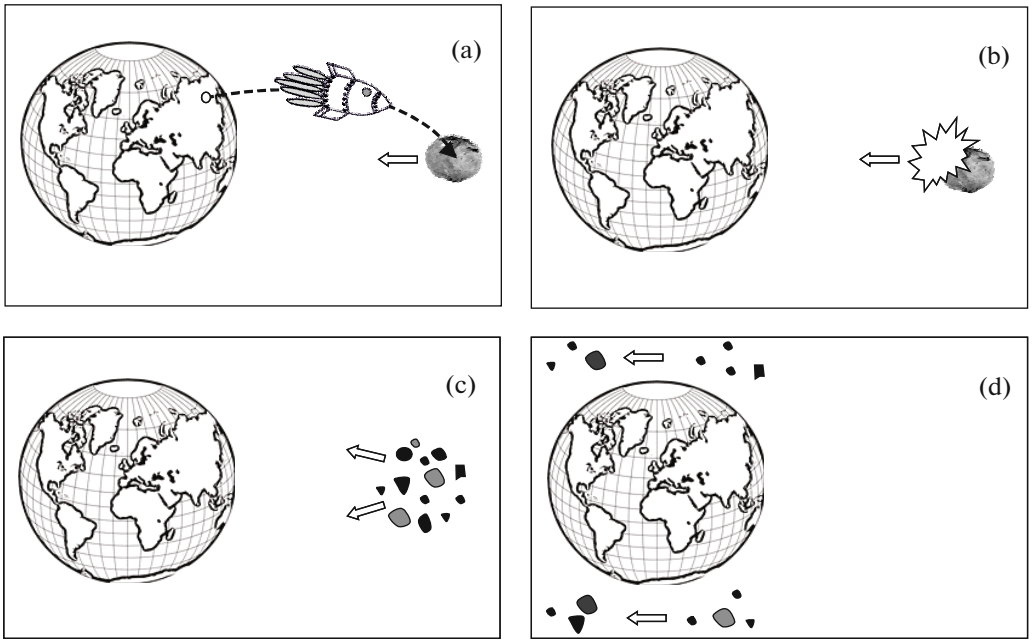

Fig. 1. The sequence of actions to prevent the asteroid hazard: (a) the detection of an asteroid, the start and flight of a rocket with a nuclear charge; (b) the nuclear explosion on the asteroid surface; (c) the asteroid fragmentation into debris of small sizes; and (d) the flight of the debris past the Earth.

tance $L = RV_{ast}/V_{frag} \approx 13$ million km from the Earth will then be required to be produced to pull apart the fragments to a distance larger than the Earth's radius $R = 6400$ km. At a mean velocity of the rocket $V_{roc} \approx 10$ km s^{-1} it must start $t = L/V_{roc} \approx 15$ days before the asteroid arrival. At this time the asteroid will be at a distance $L_1 = L(V_{ast} + V_{roc})/V_{roc} \approx 39$ million km from the Earth. A high adjustment accuracy must be provided at the entire flight stage to provide a controllable threat elimination effect. These order-of-magnitude estimates give an idea of the spatiotemporal scales for the problem being solved.

Among the methods of a destructive impact on an asteroid, a nuclear explosion [10, 11] has an overwhelming advantage over the remaining ones, because it provides a maximum specific energy release (greater than that for ordinary explosives approximately by a million times). The requirement imposed on any of the promising methods aimed at impacting an asteroid is a guaranteed elimination of the threat of a catastrophe. Thus, the development of a criterion for the deflection or destruction of an asteroid must be based on a serious conclusive foundation. Such a criterion can be determined on the basis of computational methods or using model experiments.

The full-scale elimination of the asteroid hazard using a nuclear explosion on the asteroid surface must be preceded by computational and laboratory studies, which provide an adequate interpretation of the results by taking into account the scaling effect. In this approach it is necessary to provide similar geometrical, structural, and physical (including strength) properties of the asteroid mockup and the source of impact on it.

An overall picture of the Earth's protection from the asteroid hazard using a nuclear explosion is schematically illustrated in Fig. 1.

In this paper we propose and implement a method for simulating the destructive impact of a powerful nuclear explosion on asteroids based on the principles of geometrical and physical similarity of the key gasdynamic processes and destruction processes.

We propose to replace an asteroid with a diameter of several hundred meters by a simulator (mini-mockup) with a diameter of several millimeters made of a material with the same composition and the same physical properties.

The nuclear explosion energy release is simulated by a laser pulse energy release in a small region of the mockup surface, i.e., instantaneous and point-like impacts are realized in both cases. The subject of our study is to determine the scale factor in these approaches and to work out the recommendations regarding the choice of a nuclear charge energy and the site of its effective explosion dependent on the asteroid type, size, and shape.

2. ON THE SIMILARITY OF GASDYNAMIC PROCESSES

During a nuclear explosion on the surface of an asteroid the picture of the processes as a function of time schematically appears as follows [12, 13].

The explosion energy is released in a short time interval as high-temperature radiation. In this case, about half of the energy does not hit the asteroid but is dissipated in the surrounding space as radiation and the kinetic energy of a high-velocity plasma.

The part of the energy released near the asteroid surface produces a thermal wave that rapidly propagates inward and heats up an additional mass of material. This process is accompanied by losses in the form of thermal radiation from the surface and additional high-temperature plasma expansion.

As the temperature in the region affected by the thermal wave decreases, a strong shock wave is generated in the asteroid body whose front soon overtakes the thermal wave front [12, 13]. Thereafter, the thermal energy transfer processes are damped and the shock-wave processes begin to dominate.

The area of the shock front increases, causing its amplitude to decrease. As the pressure jump at the shock front decreases to $\Delta P \approx P_0 = \rho_0 c_0^2$, the shock passes into a subsonic regime and begins to move with a speed close to the speed of sound c_0. For the chondritic material of a stony asteroid the density is $\rho_0 = 2.2–3$ g cm^{-3}, $P_0 \approx 30$ GPa, and $c_0 = 3.91$ km/s.

The heterogeneity of the asteroid structure leads to additional losses of the energy transferred by the shock and, therefore, its amplitude continues to decrease. On the other hand, subsequent "focusing," i.e., local wave amplification, can occur as the shock waves are reflected from the surface due to the curvilinear shape of the asteroid. Eventually, the dissipative processes lead to the damping of perturbations and as the pressure jump ΔP decreases to a value of the order of the ultimate strength (several MPa and tens of MPa for the tensile and compressive one, respectively), the destruction processes cease and then the fragmented asteroid is pulled apart.

The main processes at the gasdynamic stage are the propagation and interference of the sound (weak shock) waves reflected from the curved surface and the waves scattered by internal inhomogeneities. Zones of negative (disruptive) pressures are formed in these processes and the integrity of the material is undermined—the asteroid is destroyed.

The complexity of the processes and the uncertainty in the structure and shape of asteroids make accurate numerical simulations virtually impossible. Concurrently, the qualitative picture of the processes of destructive nuclear explosion impact on an asteroid described above contains obvious prerequisites for their quantitative simulations in laboratory conditions.

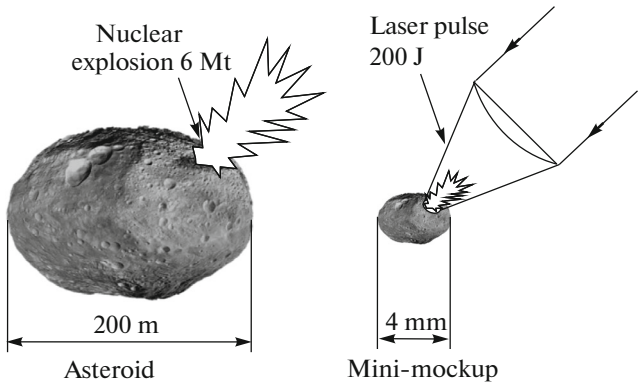

Fig. 2. A natural asteroid and a mini-mockup.

Given that, as a rule, the characteristic scale size for the condition $\Delta P \approx P_0$ to be achieved is much smaller than the sizes of hazardous asteroids, all of the stages preceding the generation of a strong acoustic wave may be considered as instantaneous and point-like ones. The short duration, the possibility of laser focusing into a small spot, the acceptable pulse energy, and the absence of an additional introduced mass make this method of simulations using laser radiation most competitive. The interpretation of this approach is demonstrated in Fig. 2.

The following is required to properly scale the problem:

(a) to fabricate a miniature mockup that has the density and strength characteristics of the asteroid, its geometrical shape, and is similar to it in all main scale sizes;

(b) to ensure that the characteristic pressures in the model and full-scale experiments are equal at the beginning of the shock-wave stage of the process. This corresponds, to within a coefficient, to the equality between the ratio of the nuclear explosion energy to the asteroid mass and the ratio of the laser energy to the mass of the simulating mini-mockup.

This coefficient is responsible for the absence of an accurate similarity of the processes at the initial stage of the full-scale and model impacts.

3. COMPUTATIONAL SUBSTANTIATION OF THE SIMULATIONS

We investigated the cases of the impact of a laser pulse on the surface of a small-size mini-mockup and a contact nuclear explosion on a full-scale asteroid in detailed gasdynamic computations by taking into account a wide range of physical processes. In our simulations we considered spherical bodies: a mockup of diameter $d_1 = 4$ mm and an asteroid of diameter $d_2 = 200$ m. The laser pulse energy was taken to be $q_1 = 200$ J. The pulse has a trapezoidal time profile with a

full width at half maximum $\tau_{0.5} = 2$ ns, the laser intensity on the plateau was $I = 2 \times 10^{14}$ W cm^{-2} at wavelength $\lambda = 0.527$ μm, and the radius of the illuminated spot was $R_1 = 125$ μm.

The nuclear explosion energy in our computations was specified from the considerations of an approximate energy similarity $d_1/q_1^{1/3} = d_2/q_2^{1/3}$ and was $q_2 =$ 6 Mt in the TNT equivalent for the chosen parameters. We assumed that for 1 t of nuclear explosive there was 1 Mt of released energy. The stylized source of energy release was an aluminum ball of radius $R_2 =$ 81 cm whose center was located on the asteroid surface, while the entire explosion energy was released in it instantaneously as heat.

The simulations of the impact of laser radiation on a mini-mockup were divided into two stages. We computed the interaction of the laser pulse with the mini-mockup material at the first stage and the subsequent gasdynamic flow of the medium by taking into account its strength properties and destruction at the second stage. The computations at the first stage were performed using the one-dimensional radiative gasdynamic SS-9M code [14] in a nonequilibrium approximation. The absorption and transfer of the laser energy by the mini-mockup were computed in a quasi-stationary wave approximation based on the solution of the Helmholtz equations by a difference method. The kinetic restriction of the electron heat conduction flux in the low-density plasma region was specified by the factor $f = 0.1$. The transfer of X-ray radiation was described in a diffusion approximation. The mean ion model was used to describe the kinetics of the ion level populations.

The one-dimensional density, internal energy, and mass velocity profiles in the mini-mockup material by the time of shock generation in the heating zone were computed with the SS-9M code. Next, using these data as the initial ones, we computed the generation and propagation of a shock wave in the entire mockup volume from the region of material heating by laser radiation with the two-dimensional EGAK code [15]. Our numerical simulations were performed in a two-dimensional axisymmetric statement on a square Euler grid. For the mini-mockup radius there were 160 computational cells (the reduced size of one computational cell was $h = 3.44$ cm kt$^{-1/3}$). Special studies showed the legitimacy of using the one-dimensional approximation to compute the initial stage of the interaction of laser radiation with the material of the asteroid mini-mockup. When varying the transition time from the one-dimensional to two-dimensional computation in the range $t_0 = 8.3$–13.8 μs kt$^{-1/3}$, the shape and amplitude of the shock wave in the loadable body barely changed at later times $t > 50$ μs kt$^{-1/3}$.

The impact of a contact nuclear explosion on a full-scale asteroid was computed with the EGAK code in an axisymmetric statement on a square Euler grid. The approximation of radiative heat conduction was used to describe the transfer of radiation through the source and asteroid materials. To save the computational resources, we considered not the entire asteroid but only its part located near the source of energy release at the thermal stage of the explosion. After the separation of the shock wave from the thermal one in the asteroid material, we took into account only the gasdynamic motion of the medium with allowance made for its strength properties and destruction. In this case, we increased the sizes of the computational domain (considered already the entire asteroid volume) and coarsened the computational grid. For the asteroid radius there were 160 computational cells (the reduced size of one computational cell was $h =$ 3.44 cm kt$^{-1/3}$).

To describe the materials of a mini-mockup and a full-scale asteroid in the range of low pressures ($P \sim$ 10 GPa), we used a generalized quasi-elastoplastic (GQEP) model of rock deformation and destruction [16] with parameters for strongly fractured granite with a density $\rho_0 = 2.4$ g cm^{-3} that was updated to be realized in the EGAK code. The shear and tearing destructions of the medium, the loosening of the fragmented material, the relaxation of stresses, and so on are taken into account in the GQED model. The equation of state [17] approximating the computations based on the Thomas–Fermi model with parameters for aluminum were used in the range of high values for the hydrodynamic parameters. The transition from the GQED model to the equation of state [18] occurred when the condition $P \geq P_{cr} = 20$ GPa was fulfilled.

Our computations showed that when the energy similarity condition is met, the nuclear explosion energy is excessive for the undeniable destruction of the asteroid. Figures 4 and 5 present the computed time dependences in the case of $q_2 = 3$ Mt for the mass velocity U and pressure P at the points marked in Fig. 3. The dimensionless coordinates of the observation points (x/d, y/d) and time tC_l/d, where $C_l =$ 3.91 km s^{-1} is the longitudinal wave speed in the material, were used in comparing the results of our computations.

There is satisfactory agreement between the model and full-scale dependences. At the remaining points the computed quantities agree similarly. Despite the huge difference in absolute scales (by a factor of 10^{14} in mass and energy), the dependences of the pressure and mass velocity on the normalized time are close in both amplitude and shape in the entire asteroid (mockup) volume. This suggests an approximate similarity of the processes and the possibility of reproducing the qualitative and quantitative features of the flow emerging during a contact nuclear explosion in laser experiments.

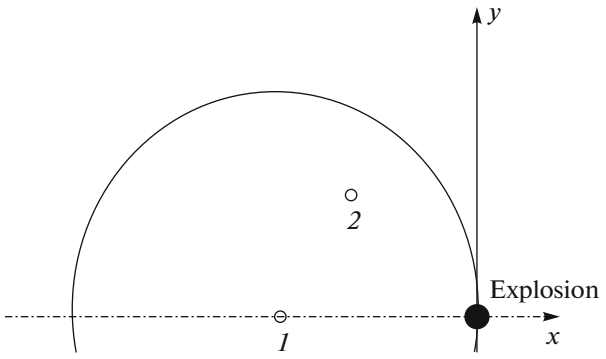

Fig. 3. Positions of the observation points in our computations.

4. ON THE TECHNOLOGY OF FABRICATING MINI-MOCKUPS FOR STONY ASTEROIDS

To carry out our laser experiments, we developed a technology of fabricating an artificial material for stony asteroids with specified properties.

The chemical compositions, densities, porosities, sound speeds, and (compressive and tensile) strengths of the mini-mockup and the asteroid must coincide to ensure their similarity.

It is also necessary to ensure the structural similarity. More specifically, there must be no big strong inclusions in the asteroid mockup that would correspond to very strong boulders absent in stony chondrites.

For the same reason, it is inexpedient to use the mini-mockups fabricated from natural chondrites, because the sizes of strong fused chondrules are comparable to the mockup sizes, breaking the similarity of the destruction processes.

The data from an analysis of the structure of the material of the stony asteroid that fell to the Earth in February 2013 near the town Chebarkul [19] formed the basis for the production of mini-mockups. The asteroid was assigned to the class of ordinary chondrites. An analysis of its debris revealed the chemical composition (SiO_2—40 wt %, MgO—26 wt %, Fe_2O_3—18 wt %, FeS—6 wt %) and some properties (a density of about 3.3 g cm^{-3}, a strength of about 9.8 MPa) of the asteroid.

When simulating the asteroid material, we chose a peculiar kind of similarity of the laboratory technologies to the natural processes of its formation in nature, i.e., we used a combination of sedimentation, compression, and heating.

The scale factor was approximately taken into account when fabricating the mockups. More specifically, we used original materials of minimal admissible dispersity. For example, the dispersity of the MgO, Fe_2O_3, and FeS powders did not exceed 20 μm, while that of SiO_2 varied within the range from 10 to 125 μm. The produced mixture was stirred in a shaking mixer for 5 h; the final packed density of the mixture was about 0.8 g cm^{-3} for all cases.

Cylindrical samples (~20 mm in diameter, ~20 mm in height) were fabricated from the prepared mixture by double-sided pressing in a closed mold on a laboratory hydraulic press. The specific pressing force was varied from 356 to 900 MPa. Using double-sided pressing improved significantly the density distribution in sample height and, as a result, the strength of the artificial asteroid material also increased [20]. The density of the model asteroid material after its pressing varied from 1.98 to 2.19 g cm^{-3}.

The samples were sintered in a vacuum under the pressure of the press in a boron nitride covering. The mold was put in a furnace and the samples were sintered under a pressure of 3.5 MPa at a temperature of 1000°C. This temperature was chosen to be below the melting temperature of the original mixture compo-

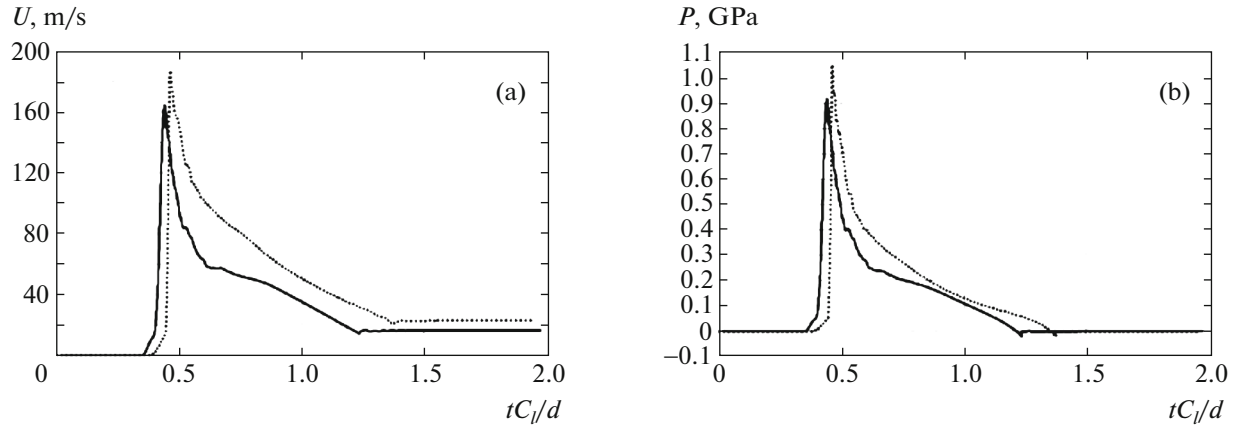

Fig. 4. Mass velocity (a) and pressure (b) versus reduced time at point *1*. The solid and dotted curves represent the laser pulse q_1 = 200 J and the contact nuclear explosion q_2 = 3 Mt, respectively.

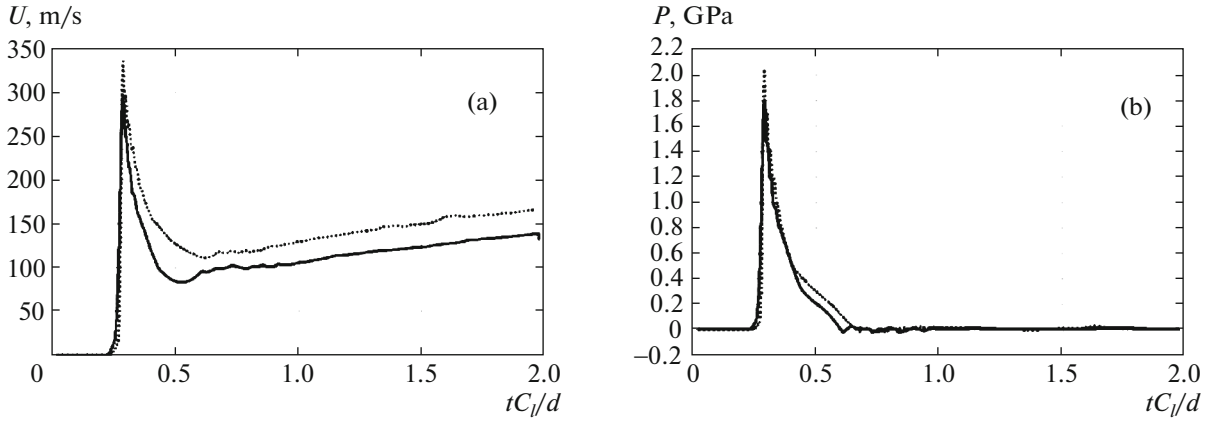

Fig. 5. Mass velocity (a) and pressure (b) versus reduced time at point *2*. The solid and dotted curves represent the laser pulse q_1 = 200 J and the contact nuclear explosion q_2 = 3 Mt, respectively.

nents. FeS has a minimum melting temperature of 1193°C.

As a result of their sintering, the samples shrank [21], while the density of the material rose approximately to 2.3 g cm^{-3}.

To study the strength characteristics of the artificial materials in each batch, we chose a check sample in each batch that was subjected to compression tests: a stress–strain relationship under sample compression similar to that in Fig. 6 was constructed from the results of our tests.

The compressive strength of the samples of artificial asteroid material fabricated with a stress under sintering of ~20 MPa was 134 MPa. The strength of the samples sintered with a stress of 3.5 MPa was 24 MPa. Despite the low density of the produced samples, their strength turned out to be fairly high. The strength of the sample sintered without any stress and covering is low, 2.7 MPa.

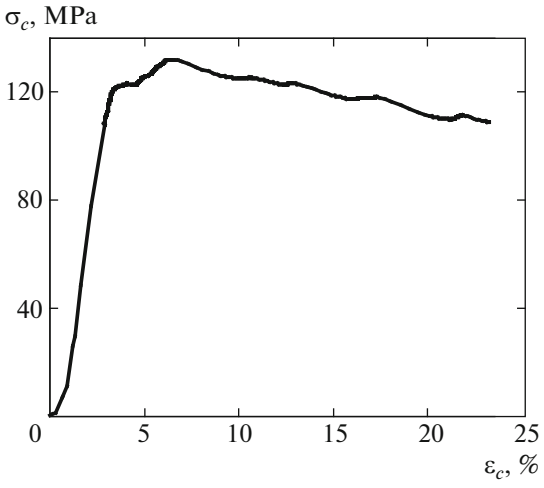

Fig. 6. Compression diagram for a sample of asteroid material with a dispersity of ~10 μm sintered at a pressure on the mold of 20 MPa.

To study the structure of the artificial asteroid material, we carried out a microscopic study of the cut of a cylindrical sample produced by a diamond cutter. We investigated the structure and determined the elemental composition of the artificial asteroid material by the methods of X-ray diffraction analysis and electron-probe X-ray spectral analysis. We investigated the structure using a backscattered electron (BSE) detector and the elemental composition using an INCA analytical attachment with an X-Max detector. The distribution of elements in the structure of the asteroid material was analyzed in the sample regions imaged at various magnifications in the regime of atomic contrast.

An analysis of the data presented in Fig. 7 and Table 1 showed the large gray particles with a size up to 300 μm to be silicon oxide, SiO_2 (region 1). The light gray region is formed by a complex oxide, $(Mg, Fe)_xO_y$ (region 2). The white region corresponds to the FeS compound (region 3). The regions whose elemental composition corresponds to the Fe_2O_3 and Fe compounds (regions 4 and 5) were also identified in the structure of the investigated material.

The phase composition of the artificial asteroid material was determined with a Dmax/RC X-ray diffractometer by the method of X-ray diffraction analysis (XDA). Our analysis showed the artificial asteroid material to be composed of three main phases: silicon oxide $SiO_2 \approx 56.1\%$, complex oxide $Mg_{1-x}Fe_xO \approx 40.2\%$, and iron sulfide $FeS \approx 3.7\%$.

Spherical samples were fabricated from the cylindrical samples of the artificial asteroid material (Fig. 8), which were subsequently used in our laser experiments to determine the criterion for the undeniable destruction of stony asteroids.

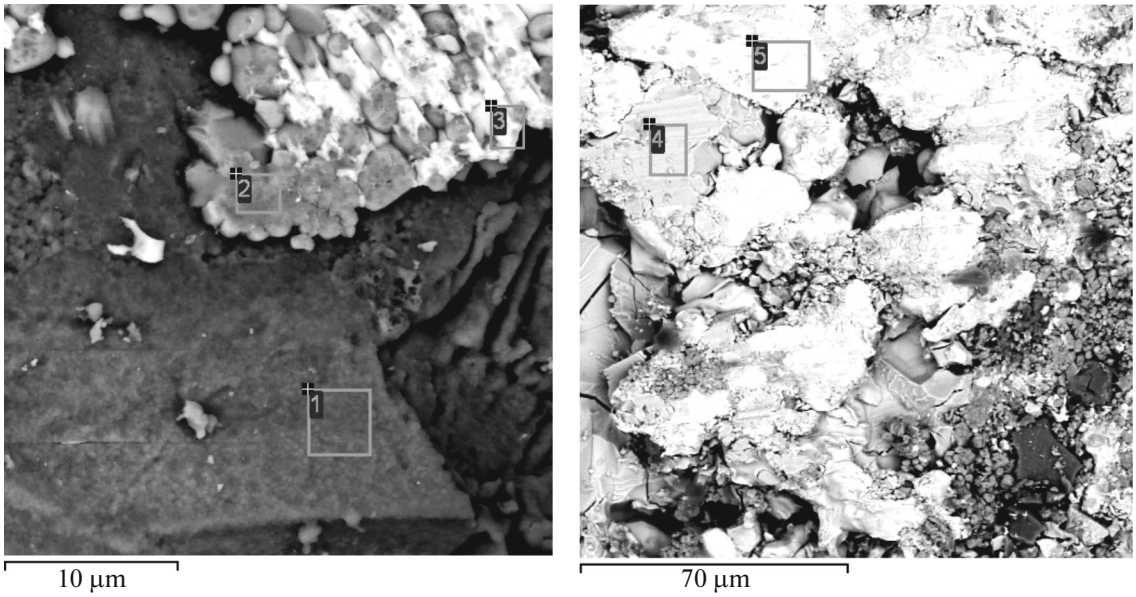

Fig. 7. Images of the regions of our microanalysis of the asteroid material.

5. LASER STUDIES

The studies were carried out at the ISKRA-5 [22], LUCH [23], and SATURN [24] laser pulse facilities.

The laser radiation from the output of the amplification channel was introduced into a vacuum chamber by a system of transport mirrors and was focused on the mini-mockup using a lens. The irradiation was done in the regime of "sharp focusing"; the spot diameter on the mockup was 100–120 μm. The designs of the experiments at different facilities differed by details. The wavelengths were 1.315 and 0.527 μm and the pulse durations were 0.4–0.6 and 1.4–2.2 ns at the ISKRA-5 and LUCH facilities, respectively. The energy varied in the range from ≈50 to ≈500 J.

The asteroid mockup was fixed on a vertically oriented holder and was placed in a special, individually adjustable box with transparent walls and a hole for the introduction of laser radiation. Thus, the possibility of lateral and rear illumination was provided to record the separation dynamics of the asteroid mockup.

A schematic diagram of the experiments at the LUCH facility and the deployment of the mockup and diagnostic systems are shown in Fig. 9; the purpose of the recording systems is presented in Table 2.

The size of the irradiation spot in our experiments was determined from its image in the X-ray radiation recorded with a pinhole camera. The imaging magnification was $M^* \approx 1.6–1.7$, the spatial resolution was 15 μm. The image was recorded using a set of filters: 10 μm Be + 23.5 μm Mylar ($C_8H_{10}O_4$) + 0.1 μm Al. The cutoff energy was about 2.6 keV.

The standard shadow method was used to record the destruction of the asteroid mini-mockup. The illumination was organized using a flash lamp with a pulse duration up to 1 ms. The images were recorded with an SER-7 electro-optical converter (EOC) [25] in a nine-frame regime. The imaging parameters are as follows:

Table 1. Elemental composition of a typical sample of chondritic asteroid material

Region number	Mass fraction, %							Probable compound
	O	F	Mg	Si	S	Ca	Fe	
1	44.6	12.5	11.3	29.0	–	1.2	1.4	SiO_2
2	31.1	–	32.6	2.3	–	–	34.0	$(Mg, Fe)_xO_y$
3	–	–	3.8	0.7	35.8	–	57.7	FeS
4	23.8	–	4.6	0.3	0.4	–	70.9	Fe_2O_3
5	–	–	1.3	–	0.7	–	98.0	Fe

Fig. 8. A spherical sample of artificial asteroid material 4.5 mm in diameter and 0.1 g in mass.

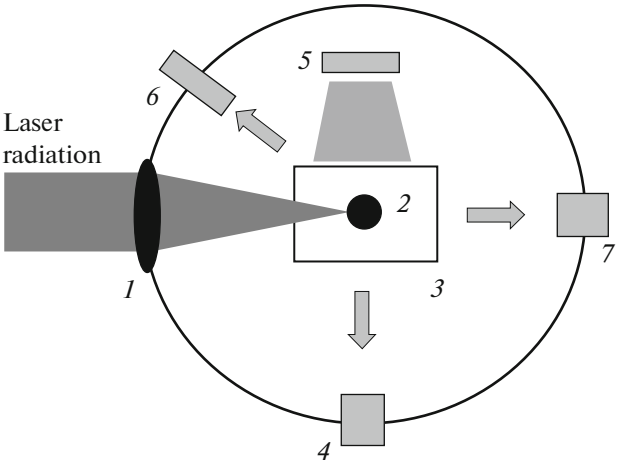

Fig. 9. Schematic diagram of the experiment at the LUCH facility: *1*—lens, *2*—asteroid mini-mockup, *3*—box with transparent walls, *4*—electro-optical converter (EOC), *5*—flash lamp, *6*—pinhole, *7*—PDV recording.

—the image region is 20–25 mm,

—the spatial resolution in the mockup region is 200 μm,

—the dynamic range is 700,

—the total imaging time is 600 μs,

—the exposure time of a single frame is 1–5 μs.

The motion of the rear side of the mini-mockup and its decay products was recorded by the Photonic Doppler Velocimetry (PDV) technique [26]. The PDV measuring system included the following:

—a narrow-band laser with a wavelength $\lambda = 1.55$ μm,

—a photodetector with a passband of 20 GHz,

—an oscilloscope with a passband of 16 GHz and 12.5-ps sampling,

—passive fiber-optic elements.

We established the fact of destruction based on a mass–dimension analysis of the debris.

To estimate the undeniable destruction criterion, we took into account the fall of the Chebarkul asteroid. This asteroid had an initial size of ~20 m and broke up into small fragments that caused no catastrophic damage when passing through the atmosphere. Thus, for an initial asteroid size of 200 m we can talk about its undeniable destruction as it broke up into debris with a linear size and a mass that are smaller than the original ones by a factor of 10 and 10^3,

Table 2. Diagnostic equipment of our experiments

Measurable parameter	Diagnostics	Measuring method
Laser radiation parameters	Standard diagnostics	Near and far zones, contrast, pulse shape, energy
Irradiation spot (size, structure)	X-ray pinhole camera	Irradiation spot image in X-ray radiation
Separation dynamics of target destruction products, debris separation diagram, debris mass and dimension characteristics, debris velocity and size distributions	Shadow recording using 9-frame "time magnifier" based on EOC	Lateral illumination of target by synchronized pulsed source
	Debris velocity measurement by PDV technique	Laser illumination of target rear side with recording of debris velocity distribution
	Sampling, analysis of debris	Target and debris weighing. Constructing histogram of debris size distribution

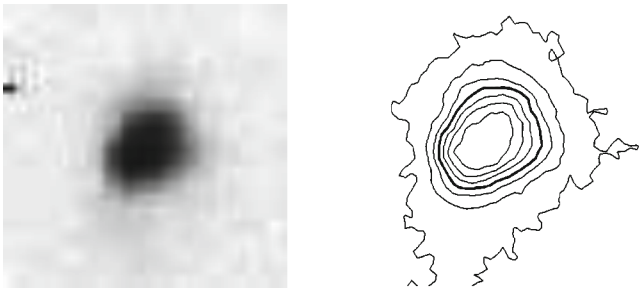

(a) (b)

Fig. 10. (a) The irradiation spot recorded with the pinhole camera and (b) isolines of its intensity distribution: the equivalent-spot diameter (FWHM) is $d_{eq} = 129$ μm.

respectively. Obviously, this estimate is valid if the trajectory of the debris in the atmosphere is close to the trajectory of the Chebarkul asteroid.

6. RESULTS OF OUR LASER EXPERIMENTS

The first simulation experiments were carried out at the ISKRA-5 facility with a laser wavelength of 1.315 μm with spherical mini-mockups. To destroy the mini-mockups of asteroids with a compressive strength of 6.5 MPa, we used laser radiation with an energy from 100 to 300 J at a pulse duration of 0.5 ns and a focusing spot of ~250 μm. In this case, the specific energy required to completely destroy the mockup was ~2000 J g^{-1}. However, the first tested mini-mockups did not satisfy the similarity criterion, because they were excessively coarse-grained (inclusions up to 800 μm in size) and weak (a compressive strength of 6.5 MPa).

In the experiments at the SATURN facility the mini-mockup shape, the targeting site, and the number of pulses per mini-mockup were varied. The laser wavelength was 1.054 μm.

The main series of experiments was carried out at the LUCH facility with a variation of the mini-mockup strength, sizes, and shape, the laser focusing method, and the number of pulses per mini-mockup. The laser wavelength was 0.527 μm.

Chondritic samples with the following parameters were used in the experiments at the LUCH facility:

—a compressive strength of 6.5, 22.5, and 140 MPa,

—a size from 3 to 10 mm,

—spherical and ellipsoidal shapes.

The beam was targeted at an ellipsoidal mockup:

—in a longitudinal direction; at the surface, into the artificial cavity, or in front of the mini-mockup surface;

—in a transverse direction: through the center or at the edge of the mockup.

For each of the irradiation cases, we carried out from 3 to 10 experiments with a variation of the energy delivered to the mockup. A total of more than 100 experiments were performed.

Figure 10 presents an image of the typical irradiation spot recorded with the X-ray pinhole camera and isolines of the intensity distribution in one of the typical experiments.

Figure 11 presents frames of the typical separation of mockup debris for one of our experiments (the case of partial destruction).

Figure 12 presents an example of recording the separation dynamics of mini-mockup debris using the PDV technique. A complete destruction of the mockup was recorded in this experiment. A single track with conserved size, velocity, and reflectivity is clearly seen in the interval 0–300 μs. The track is identified as the reflection from a compact group of aster-

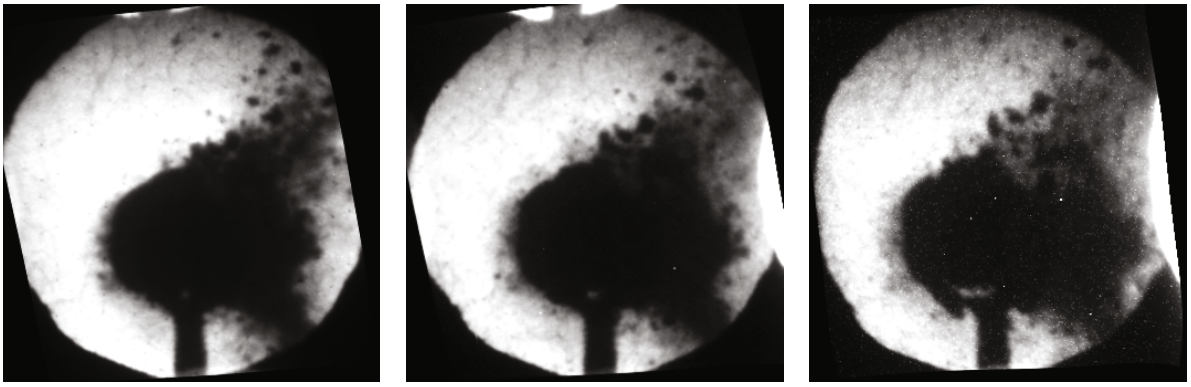

500 μs 716 μs 1006 μs

Fig. 11. Recording the asteroid mockup destruction process in the regime of nine-frame imaging (the first, fifth, and ninth frames are shown). The time is measured from the impact of laser radiation on the asteroid mockup.

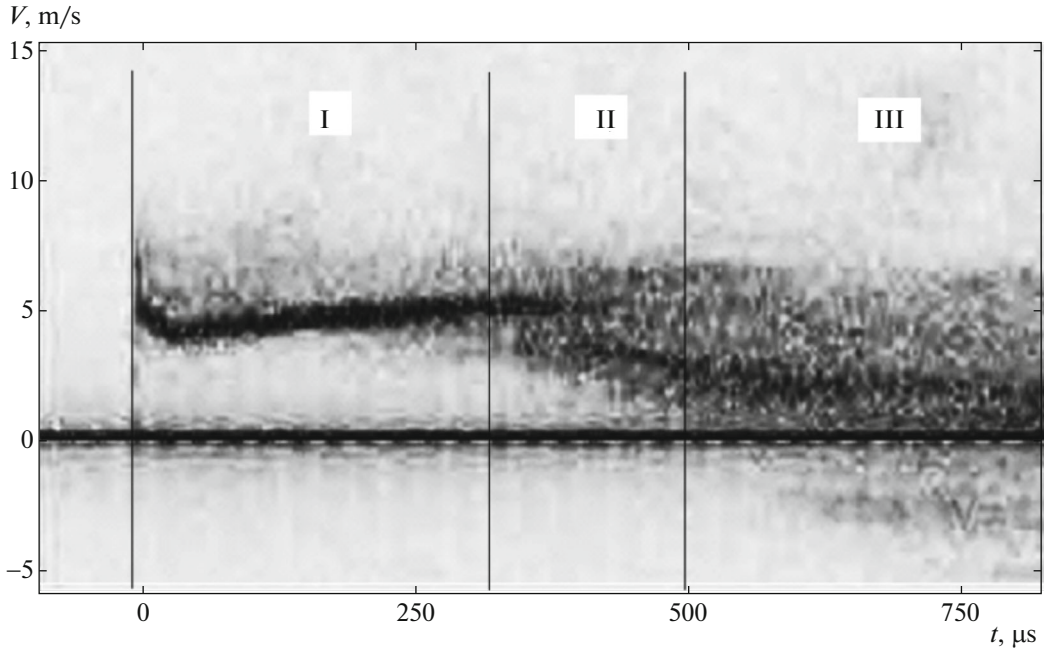

Fig. 12. Recording the motion of the mockup rear side by the PDV technique: I—the mockup moves as a whole with a velocity of 5 m s^{-1}; II—the mockup is destroyed; III—the debris move with velocities from −5 to 7 m s^{-1}.

oid mockup debris moving virtually as a single whole. Their velocity is ~5 m s^{-1}. The tracks corresponding to debris with velocities approximately from −5 (the debris fly in a direction opposite to the illumination source) to 7 m s^{-1} split up after ~300 μs. A group of debris with negative velocities appears with some delay due to their shielding by other fragments. There are separate traceable tracks of the largest particles in the instrument's field of view.

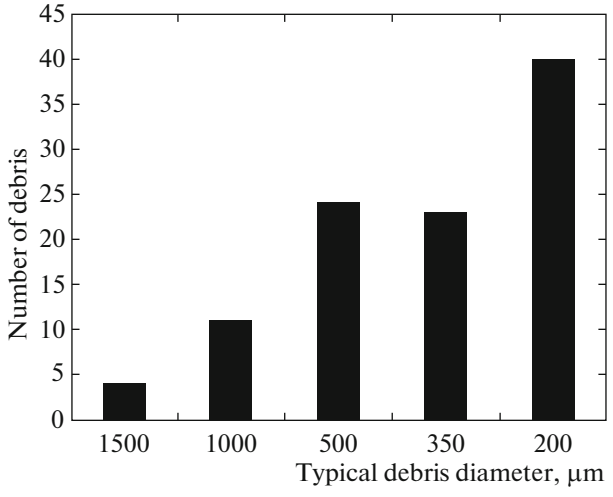

Fig. 13. The size distribution of asteroid mini-mockup debris in an experiment with a specific radiation energy of 1143 J g^{-1}.

Figure 13 presents the size distribution of coarse mini-mockup debris after the exposure to a laser pulse. We tested a mockup with a compressive strength of 6.5 MPa, a mass of 0.1050 g, and a mean diameter of 4.34 mm.

Table 3 provides detailed data characterizing the preparation and conduction stages of a typical experiment with a medium-strength mini-mockup. The results of a series of experiments (on the irradiation of samples of the same type) are presented in graphical form in Fig. 14, while the results of all our series are summarized in Fig. 15 and Table 4.

It can be seen from Fig. 14 that a chondritic mini-mockup (asteroid) is undeniably destroyed at a specific impact energy above 400–500 J g^{-1}.

It can be seen from Table 4 that for spherical mini-mockups the specific energy of their undeniable destruction increases with strength. Destruction is observed when the specific energy exceeds:

—500 J g^{-1} for mockups with a compressive strength of 6.5 MPa,

—650 J g^{-1} for mockups with a compressive strength of 22.5 MPa,

—1000 J g^{-1} for mockups with a compressive strength of 134.1 MPa.

A deviation from the spherical shape leads to an increase in the threshold specific energy. This effect is most pronounced when the impact disturbance propagates along the major axis of the mini-mockup (an approximately five-fold increase for an ellipsoid

Table 3. The type of mockup, experimental conditions, and main results

Asteroid mockup		Radiation		Result	
Compressive strength, MPa	22.5	Laser energy, J	153	Specific energy, J g^{-1}	500
Tensile strength, MPa	1.3	Laser energy on mockup, J	126	Complete destruction	no
Dispersity, μm	10–125	Duration, ns	1.6	Presence of large debris	center
Mockup diameter, mm	5.0	Contrast	$>1.5 \times 10^5$	mass of large debris, g	0.087 (35%)
Density, g cm^{-3}	2.21	Spot (pinhole) diameter, μm	171	Mass of small debris, g	0.113 (45%)
Mass, g	0.251	Laser intensity, W cm^{-2}	4.4×10^{14}	Velocity of large debris, m s^{-1}	4.5–7
Cavity	no	Targeting	center	Velocity of small debris, m s^{-1}	13

with a compressive strength of 22.5 MPa and an axial ratio of 1 : 2), see Fig. 16.

By contrast, the presence of a cavity reduces tangibly (up to 25%) the required specific energy due to its buried release.

Similar (in design) experiments were also carried out at the SATURN facility. Spherical and cubic mockups made of an analogous material with a compressive strength of 22.5 and 134 MPa were used in these experiments.

We found that the specific radiation energy required for the undeniable destruction of a mini-mockup slightly (approximately by 10%) increases with laser wavelength, because the efficiency of the laser energy conversion to the internal energy of the mockup is lower [27].

Changing the mini-mockup shape from the spherical to cubic one leads to an increase in the specific energy required to destroy the mockup approximately by 10–20%.

The pattern of destruction of mini-mockups by a sequence of laser pulses was also investigated at the SATURN and LUCH facilities. This design is fundamental for ascertaining the mechanisms of undermining the integrity of strength connections: whether the destruction effect can "accumulate" or has a threshold and whether this threshold can lower, given the preliminary impact.

Chondritic mini-mockups with a diameter of 3 mm and a compressive strength of 22.5 MPa were used to carry out these studies. The energy in the pulse was varied, while the mockups were irradiated either at the

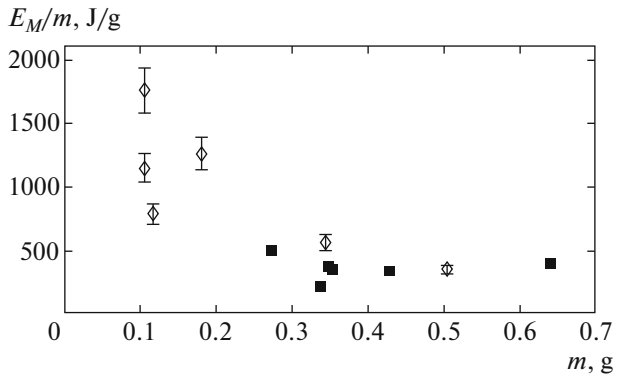

Fig. 14. Specific destruction energy of mini-mockups with a compressive strength of 6.5 GPa versus their mass. The squares and diamonds indicate the incompletely and completely destroyed mockups, respectively. The error along the vertical axis is 10%.

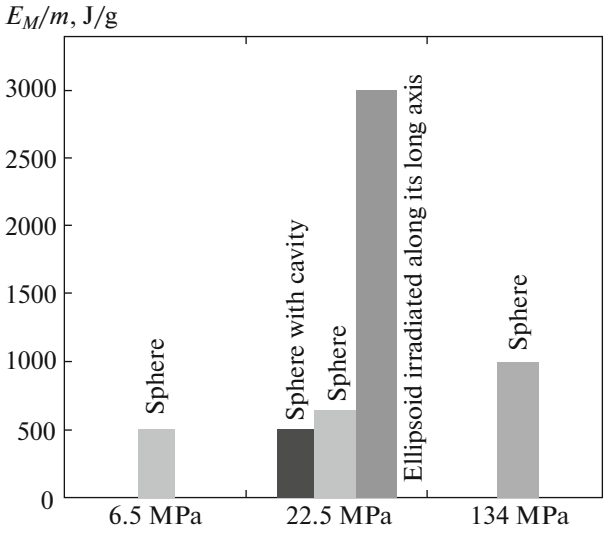

Fig. 15. The specific laser energy required to destroy mini-mockups of various shapes and strengths.

Table 4. Results of our studies of the specific energy required to destroy chondritic mini-mockups of various shapes

Mockup type and irradiation method	Mockup			Radiation		Result	
	σ, MPa	d, mm	M, g	E, J	I, 10^{14} W cm^{-2}	E/M, J g^{-1}	complete destruction
Laser radiation, M	6.5	4.4–8	0.1–0.7	70–350	2–10	200–490	no
						340–1760	yes
	134	4–5.5	0.16–0.35	120–350	1.1–12	550–1000	no
						950–1100	yes
	22.5	3–5	0.08–0.24	95–155	2.5–38	500–550	no
						450–1900	yes
Laser radiation, M	22.5	5	0.2–0.26	60–140	4.5–6	240–570	no
						530–560	yes
Laser radiation, M	22.5	3/6	0.05–0.12	50–230	1.5–9.2	390–2900	no
						2700–3000	yes
Laser radiation, M	22.5	3/6	0.07–0.11	20–190	1.1–9.6	180–400	no
						850–2400	yes

same targeting position with the formed crater from the preceding pulse or at a different one.

Our studies were performed:

– at the SATURN facility in a multiple (3–7 times) irradiation regime with a typical energy per shot from 10 to 30 J;

– at the LUCH facility in a double irradiation regime with a typical energy per shot from 100 to 200 J.

An example of the destruction of a spherical asteroid mockup by several pulses at the SATURN facility is illustrated in Fig. 17.

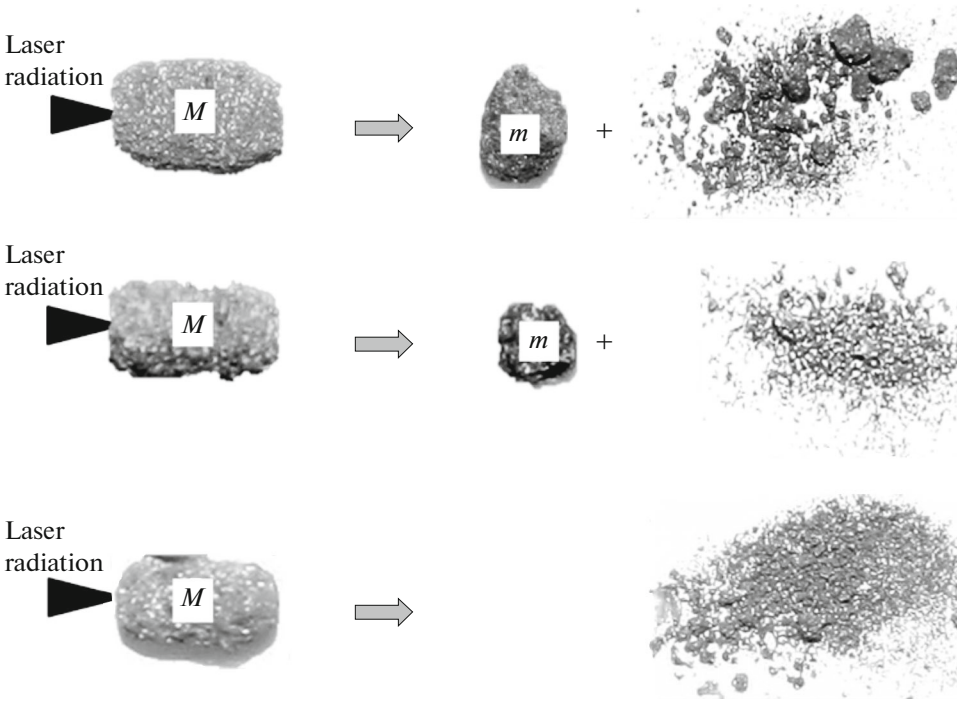

Fig. 16. The destruction of ellipsoidal mockups at various specific energies E/M: (a) $E/M = 1300$ J g^{-1}, $m = 0.45\%$; (b) $E/M = 2900$ J g^{-1}, $m = 0.23\%$; (c) $E/M = 3000$ J g^{-1}.

Fig. 17. The remnants of a spherical mockup after five shots for a focusing spot of a radius of 160 μm and a total energy $E = 51.8$ J.

In all cases, we obtained an approximate equality of the total energies required for the undeniable destruction of mini-mockups irrespective of the number and energy of single shots.

7. CONCLUSIONS

We obtained an experimental estimate of the criterion for the destruction of a chondritic asteroid by a nuclear explosion on its surface. Our studies were based on the physical similarity of the hydrodynamic phenomena accompanying the nuclear explosion on the asteroid surface and the analogous phenomena when the surface of a miniature mockup was exposed to an intense laser pulse.

The physical properties of the artificial mini-mockup material (density, porosity, strength, sound speed, etc.) were chosen to be close to those of natural chondritic asteroids.

We performed a computational–theoretical substantiation of the method of simulations using one-dimensional and two-dimensional gasdynamic computations performed in a detailed physical statement by taking into account the electron, ion, and radiative heat transfer, the equations of state for the materials in the full-scale and model cases, the absorption of laser radiation in the plasma, and a number of other processes.

We computationally estimated the influence of the initial stage of the processes on the accuracy of the gasdynamic similarity of the phenomena. We showed that at a difference in mass between the real asteroid and its laboratory analog of 14 or 15 orders of magnitude, the specific energy required for the asteroid to be completely destroyed is almost half the specific energy required for such a destruction of the mini-mockup.

To implement the program of experimental studies at several laser facilities, we created test benches to study the destruction of artificial asteroid mockups. The test benches were equipped with diagnostic tools providing the measurements of the laser radiation parameters and the parameters of its impact on the mockups.

We proposed and tried out a technique for fabricating artificial materials similar to the materials of natural chondrites. Their analysis and tests showed that the density, chemical composition, microstructure, tensile and compressive strengths, etc. are actually close to those of real asteroids. Particular attention was given to the structural similarity in order that the mockups contain no excessively large inclusions and voids that do not correspond to the structure of natural asteroids.

We performed a series of laser experiments. The undeniable destruction of spherical mini-mockups was observed if the ratio of the laser energy to the mockup mass exceeded:

—approximately 500 J g^{-1} for mockups with a strength of 6.5 MPa,

—approximately 650 J g^{-1} for mockups with a strength of 22.5 MPa,

—approximately 1000 J g^{-1} for mockups with a strength of 234 MPa.

In several experiments the laser radiation was introduced into the cavity prepared in a mini-mockup. A smaller amount of specific energy (500 J g^{-1} instead of 650 J g^{-1}) is required for the destruction of mockups under such conditions due to the greater impact efficiency of a buried explosion.

We tested ellipsoidal asteroid mini-mockups with a 1 : 2 side ratio. We showed experimentally that when an ellipsoid was irradiated along its major axis, a greater specific energy than that in the case of a spherical mockup of the same mass (3000 J g^{-1} instead of 650 J g^{-1}) is required for its destruction. No differences from the spherical case were observed when ellipsoidal mockups were irradiated transversally.

We showed that from the viewpoint of an integral destruction criterion, several weaker explosions (both simultaneous and sequential) give no noticeable advantage compared to a single explosion of the total power.

Given the scale factor and the results of laboratory experiments, the undeniable destruction of a chondritic asteroid 200 m in diameter by a nuclear explosion with an energy above 3 Mt was shown to be possible.

The works with mini-mockups of various strengths and compositions, including the mockups of stony–icy and iron–nickel asteroids, as well as the works to

refine the influence of the shape of mockups and the presence of cavities on the undeniable destruction criterion require a separate study.

REFERENCES

1. M. E. Prokhorov and A. I. Zakharov, Vestn. Sib. Aerokosm. Univ., No. 6, 118 (2011).
2. Workshop on Hearing Charter: Near-Earth Objects: Status of the Survey Program and Review of NASA's 2007 Report to Congress, Washington, DC, Nov. 8, 2007.
3. V. G. Surdin, Turin Asteroid Hazard Scale (2002). http://www.krugosvet.ru/enc/nauka_i_tehnika/astronomiya/TURINSKAYA_SHKALA_ASTEROIDNO_OPASNOSTI.html.
4. M. E. Gertsenshtein, V. V. Klavdiev, B. N. Shvilkin, et al., Nauka Tekhnol. Razrab. **89** (1), 45 (2010).
5. J. Chu, MIT News, Oct. 26 (2012). http://newsoffice.mit.edu.
6. S. Dillow, Bonnier, April 9 (2012).
7. B. Wie, Optimal Dispersion of Near-Earth Objects (NASA, 2013).
8. G. Vardaxis, T. Winkler, B. Wie, A. Pitz, and B. Kaplinger, *Conceptual Design of a Hypervelocity Asteroid Intercept* (Asteroid Deflection Res. Center, Iowa State Univ., IA, 2012).
9. Selected Abstracts of Asteroid Initiative Idea Synthesis Workshop, NASA, Nov. 20–22, 2013.
10. O. N. Shubin, Report on Round Table of Federation Council RF, March 12, 2013, Moscow; defense.council.gov.ru.
11. D. Messier, SPASE.com Contributor, May 29 (2013).
12. *Physics of Nuclear Explosion*, Vol. 1: *Explosion Development* (TsFTI MO RF, Moscow, 2000) [in Russian].
13. Ya. B. Zeldovich and Yu. P. Raizer, *Physics of Shock Waves and High-Temperature Hydrodynamic Phenomena*, Vols. 1 and 2 (Nauka, Moscow, 1966; Academic Press, New York, 1966, 1967).
14. B. A. Voinov, P. D. Gasparyan, Yu. K. Kochubei, and V. I. Roslov, Vopr. At. Nauki Tekh., Ser. Metod. Program. Chisl. Reshen. Zadach Mat. Fiz., No. 2, 39 (1993).
15. Yu. V. Yanilkin, S. P. Belyaev, A. V. Gorodnichev, A. V. Volgin, et al., Vopr. At. Nauki Tekh., Ser. Mat. Model. Fiz. Protses., No. 1, 20 (2003).
16. B. V. Zamyshlyaev and L. S. Evterev, *Models of Dynamic Deformation and Failure of Rock Masses* (Nauka, Moscow, 1990) [in Russian].
17. G. S. Collins, H. J. Melosh, and B. A. Ivanov, Meteorit. Planet. Sci. **39**, 217 (2004).
18. G. M. Eliseev and G. E. Klinishov, KIAM Preprint No. 173 (Keldysh Inst. Appl. Math., Moscow, 1982).
19. M. I. Avramenko, I. V. Glazyrin, G. V. Ionov, and A. V. Karpeev, *Calculation of Explosive Wave Parameters Caused by Chelyabinsk Bolide* (RFYaTs–VNIITF, Snezhinsk, 2013) [in Russian].
20. G. A. Vinogradov and I. D. Radomysel'skii, *Pressing and Rolling Metal-Ceramic Materials* (Mashgiz, Moscow, 1963) [in Russian].
21. S. S. Kiparisov and G. A. Libenson, *Powder Metallurgy* (Metallurgiya, Moscow, 1980) [in Russian].
22. V. I. Annenkov, V. A. Bagretsov, V. G. Bezuglov, L. M. Vinogradskii, V. A. Gaidash, I. V. Galakhov, A. S. Gasheev, I. P. Guzov, V. I. Zadorozhnyii, V. A. Yeroshenko, A. Yu. Il'in, V. A. Kargin, G. A. Kirillov, G. G. Kochemasov, V. A. Krotov, et al., Sov. J. Quantum Electron. **21**, 487 (1991).
23. N. N. Beznasyuk, I. V. Galakhov, S. G. Garanin, et al., in *Proceedings of the 4th Kharitonov's Scientific Readings* (RFYaTs–VNIIEF, Sarov, 2002), p. 82.
24. I. S. Timofeev, N. L. Aleksandrov, I. N. Burdonskiy, A. Yu. Goltsov, et al., Laser Phys. **24**, 126002 (2014).
25. A. G. Kravchenko, D. N. Litvin, V. V. Mis'ko, V. M. Murugov, A. V. Senik, and V. A. Starodubtsev, Plasma Phys. Rep. **32**, 144 (2006).
26. P. D. Sargis, N. E. Molau, D. Sweider, and M. E. Lowry, LLNL Report No. UCRL-ID-133075 (Lawrence Livermore Natl. Labor., Livermore, CA, 1999).
27. I. N. Burdonskii, A. Yu. Gol'tsov, A. G. Leonov, et al., Vopr. At. Nauki Tekh., Ser. Termoyad. Sintez **36** (2), 8 (2013).

Translated by V. Astakhov